Spin polarization of the *L*-gap surface states on Au(111)

J. Henk,* A. Ernst, and P. Bruno
Max-Planck-Institut für Mikrostrukturphysik, Weinberg 2, D-06120 Halle (Saale), Germany
(Received 23 May 2003; published 27 October 2003)

The electron spin polarization (ESP) of the *L*-gap surface states on Au(111) is investigated theoretically by means of first-principles electronic-structure and photoemission calculations. The surface states show a large spin-orbit induced in-plane ESP which is perpendicular to the in-plane wave vector, in close analogy to a two-dimensional electron gas with Rashba spin-orbit interaction. The surface corrugation, i.e., the in-plane asymmetry of the surface potential in the 1×1 unit cell, leads to a small ESP component normal to the surface. The surface-state ESP can be probed qualitatively and quantitatively by spin- and angle-resolved photoelectron spectroscopy, provided that the initial-state ESP is retained in the photoemission process and not obscured by spin-orbit induced polarization effects. Relativistic photoemission calculations provide detailed information on what photoemission setups allow one to make conclusions from the photoelectron ESP about that of the surface states.

DOI: 10.1103/PhysRevB.68.165416 PACS number(s): 73.20.At, 79.60.Bm, 71.70.Ej

I. INTRODUCTION

Spin-orbit coupling (SOC) is one of the fundamental effects in condensed-matter physics. It manifests itself in removing degeneracies in the electronic structure (spin-orbit-induced band gaps) which, for example, leads to the magnetic anisotropy in magnetic systems. Besides electronic states in the bulk, surface states can become split by SOC as well. This was shown in a pioneering photoemission investigation by LaShell *et al.*: they found that the *L*-gap surface states on Au(111) are split (in binding energy and in-plane wave vector $\vec{k}_{\parallel}$), and attributed this effect correctly to SOC.[1] Later, Petersen and Hedegård confirmed this explanation by means of tight-binding calculations.[2] These Shockley surface states are located in a bulk band gap which opens up along the Γ-*L* direction (i.e., along [111]). Being derived from *sp*-bulk states, they show an almost perfect free-electron dispersion.[3] Since the splitting is also present in the other noble metals, comparative studies on the *L*-gap surface states in Cu, Ag, and Au were performed by Hüfner's group using high-resolution photoemission[4–6] (for topical reviews, see Ref. 7 and especially Sec. 8.2 in Ref. 8). The photoemission results for Au were further corroborated experimentally by Fujita *et al.* using Fourier-transform scanning tunneling microscopy.[9] For hydrogen-covered W(110) surfaces, the spin-orbit splitting of similar surface states was also found by angle-resolved photoemission,[10] their predicted spin polarization being confirmed recently.[11]

The *L*-gap surface states can be closely related to electronic states of a two-dimensional electron gas (2DEG) in semiconductor heterostructures. In the latter, the asymmetry in direction normal to the semiconductor interface results in the so-called Rashba spin-orbit interaction.[12,13] In case of the Au surface, the asymmetry is brought about by the surface potential, in particular by the surface barrier (i.e., a vacuum-solid interface). Therefore, the *L*-gap surface states can be regarded as being subject to the Rashba effect, which might render them interesting as a model system for spintronics.[14,15]

In analogy to a 2DEG with Rashba interaction, the spin polarization of the *L*-gap surface states is assumed to lie within the surface plane and to be perpendicular to the in-plane wave vector $\vec{k}_{\parallel}$.[1] Further, the split surface states should show an opposite spin polarization. Although the *L*-gap surface states exhibit spin-orbit induced properties *par excellence*, their spin polarization was to our knowledge not investigated in detail, neither theoretically nor experimentally. Probed in a $\vec{k}$-resolved manner, for example by spin- and angle-resolved photoelectron spectroscopy (SPARPES),[8] their properties should show up unobscured by bulk transitions because they are located in a bulk band gap. However, the spin polarization of the initial state (photohole) is not necessarily that of the photoelectron, in particular if spin-orbit coupling is strong ($Z=79$ for gold). Therefore, the interpretation of spin-resolved photoemission spectra can become complicated due to the various spin-polarization effects (SPEs; for atoms, see Ref. 16). Or stated differently: on one hand, SOC produces the splitting and the spin polarization of the surface states. On the other hand, it may prevent one from probing the latter by means of SPARPES because of the SPEs.

The purpose of the present paper is twofold. First, *ab initio* electronic-structure calculations provide detailed information on the properties of the *L*-gap surface states, in particular on their dispersion and spin polarization. These results are compared to those for a two-dimensional electron gas with Rashba spin-orbit interaction. Second, we address the question whether and how the surface-state spin polarization can be probed by SPARPES. State-of-the-art photoemission calculations for a variety of setups show how the SPEs affect the photoelectron spin polarization. Former studies of the photoelectron spin polarization from nonmagnetic surfaces were performed for normal emission. For Au(111), the photoelectrons are to be detected in off-normal emission (due to the dispersion of the surface states) which leads for some setups to distinguished spin-dependent photoelectron diffraction effects. Questions to be answered comprise the degree and orientation of the spin polarization as well its dependence on the wave vector $\vec{k}_{\parallel}$.

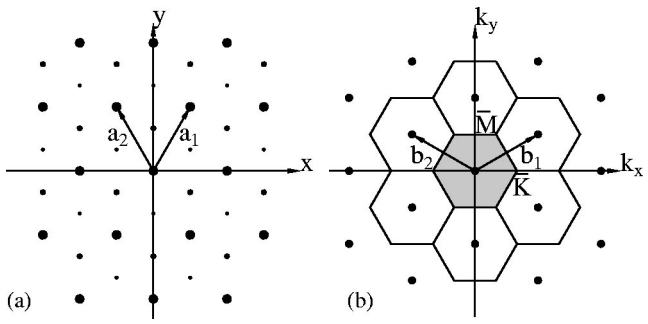

FIG. 1. The Au(111) surface. (a) Top view of the first three surface layers (first, second, and third layer: large, medium-sized, and small filled circles, respectively). $\vec{a}_1$ and $\vec{a}_2$ are the basis vectors of the direct lattice. The z axis points towards the bulk. (b) Two-dimensional reciprocal lattice with basis vectors $\vec{b}_1$ and $\vec{b}_2$. The first Brillouin zone is marked gray. The two representative symmetry points $\bar{\mathrm{K}}$ and $\bar{\mathrm{M}}$ mark a corner $[\vec{k}_\parallel(\bar{\mathrm{K}})=(\vec{b}_1-\vec{b}_2)/2]$ and a center $[\vec{k}_\parallel(\bar{\mathrm{M}})=(\vec{b}_1+\vec{b}_2)/2]$ of the Brillouin-zone boundary, respectively.

This paper is organized as follows. In Sec. II, theoretical aspects and relevant details of the computations are presented. Section III focuses first on the analogy between the electronic states in a 2DEG (Sec. III A) and the *L*-gap surface states. The properties of the surfaces states are discussed in Sec. III B, in particular the dispersion (Sec. III B 1) and the spin polarization (Sec. III B 2). The theoretical photoemission results are eventually presented in Sec. III C.

II. COMPUTATIONAL ASPECTS

A. Au(111) surface

The Au(111) surface is shown schematically in Fig. 1(a). The x axis corresponds to the crystallographic $[1\bar{1}0]$ direction, whereas the y axis is along $[\bar{1}\bar{1}2]$.

In the present work, only the 1×1 unit cell is considered. The so-called herringbone reconstruction with a $22\times\sqrt{3}$ unit cell will not be addressed.[17] The main effect of this surface modification is a modulation of the surface-state photoemission intensities due to backfolding (surface *umklapp*).

B. *Ab initio* electronic-structure calculations

The electronic structure of the Au(111) surface was computed from first-principles using the local-density approximation (LDA) of density-functional theory with the Perdew-Wang exchange-correlation potential.[18] The Korringa-Kohn-Rostoker (KKR) method was applied to semi-infinite systems, hence avoiding slab geometries.

Within our KKR scheme (for details, see Ref. 19), we computed first the bulk muffin-tin potentials. Subsequently, the potentials of the outermost six Au surface layers and the three vacuum layers were calculated self-consistently for the semi-infinite system. The Au layers were not relaxed (ideal surface) but for the vacuum layers an outward relaxation of 4% (compared to the bulk interlayer distance) was assumed. The latter improved the dispersion of the surface states in comparison to the experimental findings significantly (this procedure clearly reveals shortcomings of the muffin-tin approximation for the potential, the latter being avoided in full-potential methods). The work function of 5.23 eV agrees well with the experimental value of 5.31 eV.[8]

The *ab initio* calculations provide details of the electronic structure by means of the layer- and wave-vector-resolved spectral density,

$$N_l(E,\vec{k}_\parallel)=-\frac{1}{\pi}\mathrm{Im}\,\mathrm{Tr}\,G^+_{ll}(E,\vec{k}_\parallel), \tag{1}$$

where the trace Tr is over a muffin-tin sphere of layer l and $G^+_{ll}(E,\vec{k}_\parallel)$ is the + side limit of the layer-diagonal Green function at energy E and wave vector $\vec{k}_\parallel=(k_x,k_y)$ (Cartesian coordinates are defined in Fig. 1).[20] A further decomposition of N_l with respect to spin and angular momentum gives access to the relevant surface-state properties.

To investigate the effect of spin-orbit coupling on the *L*-gap surface states, we scaled the SOC strength by interpolating between the fully relativistic and the scalar-relativistic case.[21,22] Therefore, only SOC is scaled whereas the other relativistic effects remain unchanged (note that this is advantageous compared to scaling the velocity of light c). We would like to note that this scheme applies only for the muffin-tin spheres, leaving the gradient of the surface potential almost unaffected.

C. Photoemission calculations

The photoemission calculations were performed using the `omni2k` computer program for electron spectroscopies,[23] and rely on the one-step model as being formulated in the spin-polarized relativistic layer-KKR method.[24,25] Therefore, spin-orbit coupling is included in a natural way by solving the Dirac equation. This is in particular important because the SOC-induced photoelectron spin polarization is fully taken into account. The self-consistent potentials from the *ab initio* calculations serve as input, putting electronic-structure and photoemission results on equal footing.

The `omni2k` computer program proved to be successful in a number of investigations (see Ref. 26 for further publications). In particular, spin-orbit effects from nonmagnetic surfaces were described quantitatively [for theoretical predictions of spin-polarization effects with linearly polarized light (see Refs. 27, 28, and 29); all these effects were confirmed experimentally by Heinzmann's group[30–32]], but also the closely related magnetic dichroism was addressed correctly.[33–36] Hence, we expect that both the photoemission intensities and the spin polarizations presented in Sec. III C agree well with future experiments on Au(111).

The inverse lifetimes of the photohole (at energies close to the Fermi level) and of the photoelectron (at about 15 eV kinetic energy) were chosen as 0.015 and 1.25 eV, respectively. The maximum angular momentum was $l_{\max}=4$ and the sum over layers comprised the first 30 layers. Metal optics were taken into account via Fresnel's equations and Snell's law.

In the following, the incidence direction of the light is described by a polar angle $\vartheta_{\rm ph}$ and an azimuth $\varphi_{\rm ph}$. The in-plane component of the photoelectron wave vector is given by

$$\vec{k}_{\parallel}=\sqrt{2E_{\rm kin}}\sin\vartheta_{\rm e}\begin{pmatrix}\cos\varphi_{\rm e}\\ \sin\varphi_{\rm e}\end{pmatrix}, \tag{2}$$

where $E_{\rm kin}$ is the kinetic energy. For the $\overline{\Gamma}$-$\overline{\rm M}$ direction in the two-dimensional Brillouin zone one has for example $\varphi_{\rm e}=90°$, and for $\overline{\Gamma}$-$\overline{\rm K}$ $\varphi_{\rm e}=0°$ [Fig. 1(b)].

III. DISCUSSION AND RESULTS

A. Rashba spin-orbit interaction in a two-dimensional electron gas

Time-reversal symmetry requires for the dispersion relation $E(\vec{k}_{\parallel},\tau)=E(-\vec{k}_{\parallel},-\tau)$, where $\tau=\uparrow,\downarrow$ is the electron spin. Inversion symmetry (which is present in the bulk of cubic lattices) implies $E(\vec{k}_{\parallel},\tau)=E(-\vec{k}_{\parallel},\tau)$. Combining these relations yields $E(\vec{k}_{\parallel},\tau)=E(\vec{k}_{\parallel},-\tau)$ (Kramers' degeneracy) which states that the electronic states in the bulk are not spin-polarized. However, the presence of a surface breaks the inversion symmetry and, hence, a spin-orbit-induced splitting accompanied by a nonzero spin polarization is permitted. As Petersen and Hedegård pointed out, the splitting depends on both the size of the atomic SOC and of the gradient of the surface potential.[2]

Spin-orbit terms linear in the wave vector $\vec{k}$ occur in the Hamiltonian due to a symmetry reduction of the system (heterostructure, film, and surface) with respect to the corresponding bulk system (for a review, see Ref. 37). Particularly important is the structural inversion asymmetry which occurs typically at semiconductor interfaces (e.g., in a two-dimensional electron gas),[38] but in fact needs not to be related to the crystal structure. In this case, the linear $\vec{k}_{\parallel}$-terms are the so-called Rashba terms.[12,13] As will be motivated in the following, there exists a close analogy between the spin-orbit split electronic states in a 2DEG and the *L*-gap surface states at (111) surfaces.

Spin-orbit coupling in a crystal with potential $V(\vec{r})$ is described by

$$H_{\rm so}=\frac{1}{2c^2}\vec{s}\cdot(\vec{\nabla}V\times\vec{p}), \tag{3}$$

where $\vec{s}$ is the spin and $\vec{p}$ the momentum operator.[39] In a 2DEG, V is invariant parallel to the semiconductor interface, leading to $V=V(z)$. Hence, one can describe the system by the free-electron Hamiltonian $\vec{p}^{\,2}/2$ in two dimensions [xy plane, $\vec{\rho}=(x,y)$] including $H_{\rm so}$. This results in the Schrödinger equation

$$\left[\frac{1}{2}\vec{k}_{\parallel}^{2}\mathbf{1}+\gamma_{\rm so}(\boldsymbol{\sigma}_x k_y-\boldsymbol{\sigma}_y k_x)\right]\Psi=E\Psi, \tag{4}$$

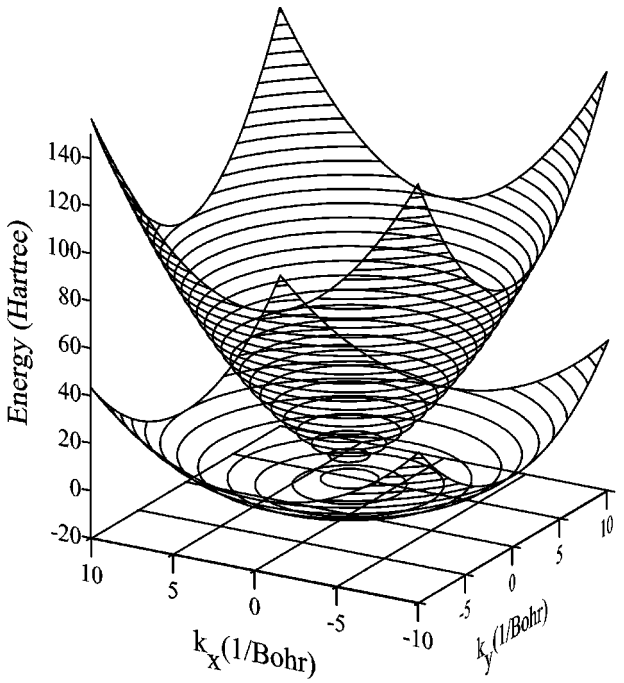

FIG. 2. Rashba spin-orbit interaction in a two-dimensional electron gas. The dispersions $E_{\pm}(\vec{k}_{\parallel})$ of free electrons are shown for $\gamma_{\rm so}=4$/Bohr, $\vec{k}_{\parallel}=(k_x,k_y)$. The "inner" state ["+" in Eq. (6)] shows strong dispersion, the "outer" weak dispersion ["−" in Eq. (6)]. Both surfaces touch each other at $\vec{k}_{\parallel}=0$. For a better illustration, the Rashba effect is extremely exaggerated (compared to typical two-dimensional electron gases).

where bold symbols represent 2×2 matrices, e.g., the Pauli matrices $\boldsymbol{\sigma}_i$, $i=x,y,z$. The parameter $\gamma_{\rm so}$, which is assumed positive and is related to the derivative of $V(z)$, controls the strength of the Rashba spin-orbit interaction. The above equation is solved by the *ansatz*

$$\Psi(\vec{\rho},\vec{k}_{\parallel})\propto\exp(i\vec{k}_{\parallel}\cdot\vec{\rho})(\pi_{\uparrow}\chi^{\uparrow}+\pi_{\downarrow}\chi^{\downarrow}) \tag{5}$$

for the wave functions (for details, see Ref. 2). The Pauli spinors $\chi^{\uparrow}$ and $\chi^{\downarrow}$ are quantized along the z axis.

The eigenvalues $E_{\pm}$ of Eq. (4) are given by free-electron parabolae that are shifted in $\vec{k}_{\parallel}$:

$$E_{\pm}=\frac{1}{2}k_{\parallel}^{2}\pm\gamma_{\rm so}|\vec{k}_{\parallel}|. \tag{6}$$

The + solution gives rise to an "inner" paraboloidlike surface (strong dispersion in Fig. 2), the − solution to an "outer" one (weak dispersion in Fig. 2).

The associated eigenfunctions $\Psi_{\pm}$ are fully spin polarized, as is evident from the spin polarization

$$\vec{P}_{\pm}(\vec{k}_{\parallel})=\frac{1}{|\vec{k}_{\parallel}|}\begin{pmatrix}\pm k_y\\ \mp k_x\\ 0\end{pmatrix}=\begin{pmatrix}\pm\sin\varphi_{\rm e}\\ \mp\cos\varphi_{\rm e}\\ 0\end{pmatrix}, \tag{7}$$

with $\vec{k}_{\parallel}=|\vec{k}_{\parallel}|(\cos\varphi_{\rm e},\sin\varphi_{\rm e})$ [cf. eq. (2)]. The spin polarization is perpendicular to $\vec{k}_{\parallel}$, with P_{+} (P_{-}) rotating clockwise

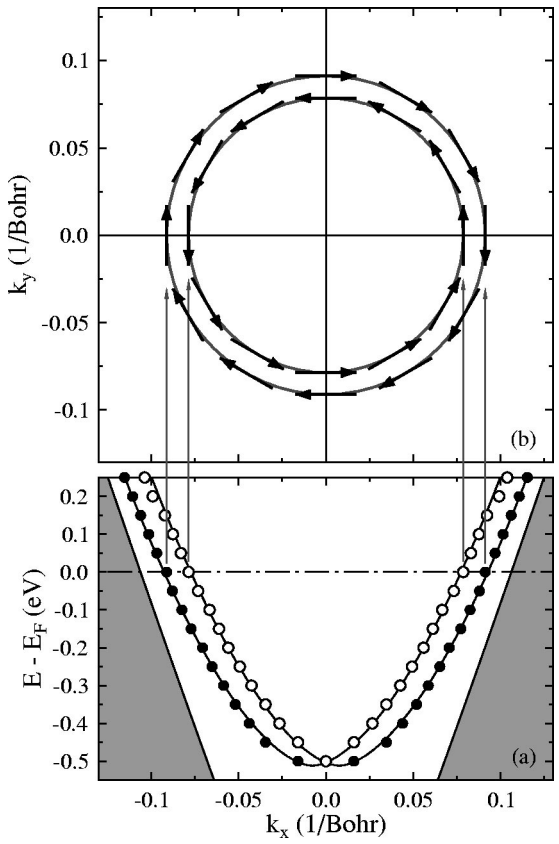

FIG. 3. *L*-gap surface states on Au(111). (a) Dispersion of the spin-orbit split surface states along $\overline{\mathrm{K}}$-$\overline{\Gamma}$-$\overline{\mathrm{K}}$ [i.e., $\vec{k}_\parallel=(k_x,0)$]. Open (closed) symbols belong to the inner (outer) surface state. Gray arrows point from the surface states at the Fermi energy E_F to the momentum distribution shown in panel b. The region of bulk bands is depicted by gray areas. (b) Momentum distribution at E_F. The thick arrows indicate the in-plane spin polarization [P_x and P_y, according to Eq. (9)].

(anticlockwise) around the z axis. P_z vanishes, for the inversion asymmetry being exclusively along the z direction. At $\vec{k}_\parallel=0$, the states are degenerate and the electron spin polarization becomes zero [$E_+=E_-=0$ and $\vec{P}_+ + \vec{P}_- = 0$].

B. Properties of the *L*-gap surface states

1. Dispersion

The dispersion of the surface states was obtained from the maxima in the layer- and wave-vector-resolved spectral density [Eq. (1)] and is shown in Fig. 3(a). The minimum energy is -0.51 eV which agrees well with the experimentally observed value of -0.49 eV and with that of an FLAPW (full-potential linearized augmented plane wave) calculation.[6] However, our theory gives a stronger dispersion than the experiment: the Fermi wavenumbers $k_\mathrm{F}^\mathrm{in}=0.079$/Bohr and $k_\mathrm{F}^\mathrm{out}=0.091$/Bohr for the inner and the outer surface states, respectively, are slightly too small compared to the experimental values of 0.091/Bohr and 0.104/Bohr [FLAPW calculations with the WIEN code gave the same trend.[6] It can probably be related to the LDA surface barrier which is in general to steep compared to an image-potential barrier. The trend is furthermore consistent with energy-dependent surface barriers that were introduced to describe correctly image-potential states on Pd(110): these barriers became smoother with increasing electron energy[40]]. The spin-orbit splitting (in $\vec{k}_\parallel$) agrees well: 0.012/Bohr (theory) to 0.013/Bohr (experiment), hence corroborating that the important surface-state properties are well described by our theory.

In semiconductor 2DEGs, the spin-splitting energy at zero magnetic field is typically in the order of a few meV (e.g., 2.5–3.5 meV from Refs. 41 and 42). The corresponding values for the spin-orbit coupling γ_so, as obtained from Shubnikov–de Haas oscillations, range from about 0.7×10^{-9} eV cm (Refs. 43 and 44) to 0.9×10^{-9} eV cm (Refs. 41 and 38). The Rashba effect appears to be considerably larger for the Au(111) surface: the spin-splitting energy of about 0.14 eV corresponds to a γ_so of about 4.4×10^{-9} eV cm. More predicative in this context is the relative $k_\parallel$ splitting $\Delta k_\mathrm{F}=2(k_\mathrm{F}^\mathrm{out}-k_\mathrm{F}^\mathrm{in})/(k_\mathrm{F}^\mathrm{out}+k_\mathrm{F}^\mathrm{in})$, which equals about 14% for Au(111). For a 2DEG, this quantity is directly related to the carrier densities of the spin-split states, resulting in $\Delta k_\parallel \approx 4\%$ (Ref. 41). We note in passing that the splitting of the *sp*-derived states on Au(111) is less than that for comparable *d*-derived surface states on W(110),[45] possibly due to the increase of SOC with angular momentum ($H_\mathrm{so} \propto \vec{l}\cdot\vec{\boldsymbol{\sigma}}$ for a central potential).

In accord with Eq. (6), the momentum distributions (MDs) at the Fermi energy E_F are concentric circles [Fig. 3(b)], confirming the nomenclature of an inner and outer surface state (cf. also the constant-energy cuts in Fig. 2). One would expect that the symmetry of the surface would produce deviations of the MDs from the circular shape. By checking carefully the spectral density, we found indeed tiny deviations which, however, are by far too small to be observable even in high-resolution photoemission experiments. Therefore, we regard the MDs as circular.

2. Spin polarization at the Fermi energy

Taking into account the point group $3m$ of the (111) surface, the crystal potential in Eq. (3) can be written in cylinder coordinates [$\vec{r}=(\rho,z,\varphi)$] as

$$V(\vec{r}) = V_0(\rho,z) + V_3(\rho,z)\sin 3\varphi + V_6(\rho,z)\cos 6\varphi + \cdots . \tag{8}$$

In analogy to the derivation for a 2DEG [Sec. III A, with $V(\vec{r})=V_0(z)$] and by considering time-reversal symmetry, the leading terms in φ_e [Eq. (2)] of the electron spin polarization (ESP) at a fixed energy are given by

$$\vec{P}(\varphi_\mathrm{e}) = \begin{pmatrix} \alpha\sin\varphi_\mathrm{e} \\ -\alpha\cos\varphi_\mathrm{e} \\ \beta\cos 3\varphi_\mathrm{e} \end{pmatrix}. \tag{9}$$

Hence, the spin polarization rotates clockwise (anticlockwise) for $\alpha>0$ ($\alpha<0$) around the z axis (surface normal). Evidently, the net spin polarization at the surface is zero and the system remains nonmagnetic. Further, the signs for α of

the two spin-split surface states should be opposite, $\mathrm{sgn}(\alpha^{\mathrm{in}}) = -\mathrm{sgn}(\alpha^{\mathrm{out}})$ [vanishing SOC requires that $\vec{P}(\vec{k}_{\parallel}) = 0$ if summed over both states; that is $\alpha^{\mathrm{in}} = -\alpha^{\mathrm{out}}$]. The nonzero P_z reflects directly the threefold symmetry of the surface. In particular, $|P_z|$ is largest at integer multiples of $\varphi_e = n \times 60°$, n integer, that is in the directions of the first-nearest-neighbor atoms within the surface layer (Fig. 1). To our knowledge, the ESPs, in particular the modulus and signs of α^{in} and α^{out} as well as of β^{in} and β^{out}, were not addressed in detail up to now, in particular with respect to the 2DEG results (Sec. III A). For the latter, we obtained $\alpha^{\mathrm{in}} = +1$ (+100%) and $\alpha^{\mathrm{out}} = -1$ (−100%) [Eq. (7)]. Further, β^{in} and β^{out} vanish.

The spin polarization of the surface states is due to the gradient of the surface potential, which plays the role of the inversion asymmetry in a 2DEG. The z derivative is much larger than the in-plane derivatives that are related to the surface-potential corrugation, i.e., the in-plane asymmetry of the surface potential. Therefore, $|\alpha| \gg |\beta|$ is expected. Indeed, the spin-resolved spectral densities of the outermost Au layer at the Fermi energy gave $\alpha^{\mathrm{in}} \approx -96.7\%$ and $\alpha^{\mathrm{out}} \approx +92.6\%$, whereas $\beta^{\mathrm{in}} \approx -1.4\%$ and $\beta^{\mathrm{out}} \approx +1.3\%$. Comparing these results with Eq. (7) suggests that the Rashba parameter γ_{so} is negative for the Au(111) surface, since a positive γ_{so} corresponds to $\alpha^{\mathrm{in}} > 0$ and $\alpha^{\mathrm{out}} < 0$. The large in-plane spin polarization is consistent with spin-resolved photoemission experiments on W(110)-(1×1)H that report on 100% ESP, with regard to experimental resolution and statistics (see Fig. 2 in Ref. 11).

That the surface states are not fully spin-polarized, as is the case for the 2DEG [cf. Eq. (7)] is a further manifestation of the crystal structure of the (111) surface. In order to investigate this finding, we concentrated on the $\bar{\Gamma}$-$\bar{\mathrm{M}}$ direction (that is, $\varphi_e = 90°$ to obtain $P_z = 0$) and scaled the spin-orbit interaction Sec. II B). For vanishing SOC, the surface-state wave functions are pure Pauli spinors and their spatial parts are degenerate. Hence, $\alpha_{\mathrm{in}} = -\alpha_{\mathrm{out}}$ and $\beta_{\mathrm{in}} = -\beta_{\mathrm{out}}$, and the net ESP at a certain $\vec{k}_{\parallel}$ consequently vanishes. With increasing SOC, and hence increasing splitting, each wave function gets an admixture of the other spin orientation. Furthermore, the spatial parts of the wave functions are no longer degenerate. In other words, the difference in $|\alpha^{\mathrm{in}}|$ and $|\alpha^{\mathrm{out}}|$ can be attributed to the different ''locations'' in the two-dimensional Brillouin zone of the SOC-split surfaces states.

This finding is supported by the layer- and spin-resolved spectral density of the surface states integrated over the muffin-tin spheres [Eq. (1)]. The spectral weight extends considerably into the bulk (about 12 layers; see Fig. 4), in agreement with recent calculations using a slab geometry.[6] The most striking fact, however, is that both inner and outer surface states decay differently towards the bulk and do not show a full spin polarization (Note that the only nonzero ESP component along $\bar{\Gamma}$-$\bar{\mathrm{M}}$ is P_x, due to symmetry reasons). The spin polarization decreases (in absolute value) towards the bulk, providing evidence of the surface origin of the spin-orbit induced splitting.

Summarizing at this point, the properties of the *L*-gap surface states show a close correspondence to those of the electronic states in a 2DEG with Rashba spin-orbit interaction. The crystal structure of the (111) surface leads, in particular, to a slightly reduced degree of spin polarization and to a nonzero but small P_z. Further, crystal properties show up in different degrees of localization for the inner and the outer surface state.

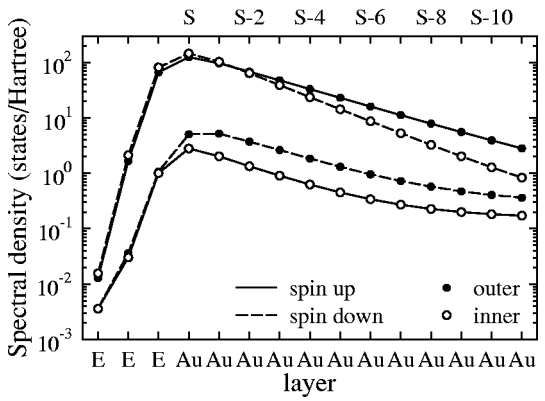

FIG. 4. Layer- and spin-resolved spectral density of the surface states at the Fermi energy. The wave vectors are along $\bar{\Gamma}$-$\bar{\mathrm{M}}$ [$\vec{k}_{\parallel} = (0, k_{\mathrm{F}}^{\mathrm{in}})$ and $(0, k_{\mathrm{F}}^{\mathrm{out}})$, respectively]. ''E'' and ''Au'' denote vacuum and Au layers, respectively. ''S'' and ''S-2'' give the standard nomenclature for surface layers, starting with the outermost Au layer ''S.'' The terms ''spin up'' and ''spin down'' refer to P_x [cf. Eq. (9) with $\varphi_e = 90°$]. Note the logarithmic scale of the abscissa.

C. Probing the spin polarization by photoelectron spectroscopy

1. Spin-polarization effects in photoemission

Depending on the photoemission setup, one can easily produce spin-polarized photoelectrons from a nonmagnetic surface, an effect mainly due to spin-orbit coupling in the initial states. For circularly polarized light, the effect is commonly termed ''optical orientation'' because the photoelectron spin is aligned along the incidence direction of the light while its orientation is determined by the light helicity.[46] For linearly polarized light, different effects were theoretically predicted and experimentally confirmed (see references given in Sec. II C).

The major aspect for producing spin-polarized photoelectrons from a nonmagnetic surface is the symmetry of the entire setup which comprises the crystal surface, light polarization and incidence direction as well as the electron-detection direction. As a rule of thumb, one can assume that the less symmetry, the more components of the photoelectron ESP are nonzero. In order to reliably probe the spin polarization of an initial state (here an *L*-gap surface state) one has to assure that only those components of the photoelectron ESP are nonzero that are also nonzero for the initial state. This restriction implies that one has to choose the ''correct'' photoemission setups. Otherwise, it might be difficult—if not impossible—to conclude from the photoelectron ESP on that of the initial state. The main complication in probing the ESP of the *L*-gap surface states arises from the indispensable off-normal emission of the photoelectrons. It reduces the sym-

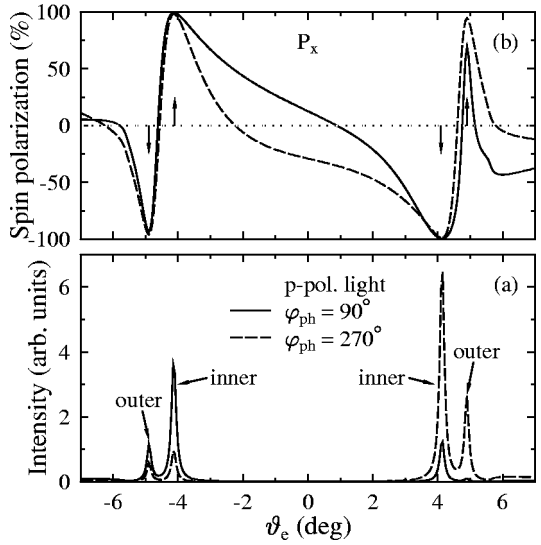

FIG. 5. Spin-resolved photoemission for $\vec{k}_\parallel$ along $\overline{\mathrm{M}}$-$\overline{\Gamma}$-$\overline{\mathrm{M}}$ ($\varphi_e = 90°$) and *p*-polarized light ($\omega = 21.22$ eV, $\vartheta_{ph} = 45°$). (a) Intensities for $\varphi_{ph} = 90°$ (solid) and 270° (dashed) azimuth of light incidence. The surface-state maxima are indicated (''inner'' and ''outer''). (b) Associated photoelectron spin polarization along $\vec{x}$. The vertical arrows mark the positions of the surface states.

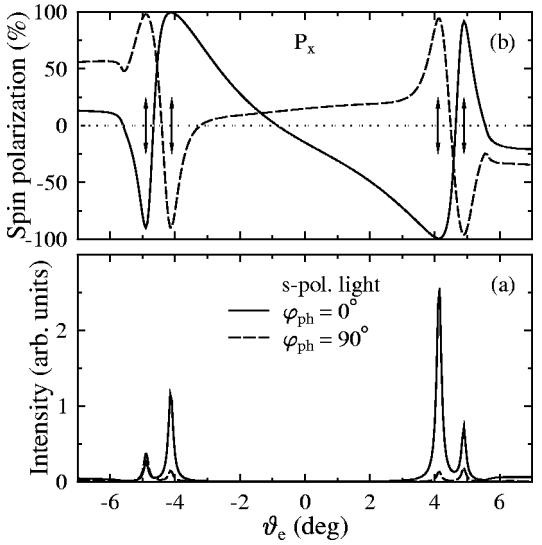

FIG. 6. As Fig. 5 but for *s*-polarized light ($\omega = 21.22$ eV). (a) Intensities for $\varphi_{ph} = 0°$ (solid) and 90° (dashed) azimuth of light incidence. (b) Associated photoelectron spin polarization along $\vec{x}$.

metry considerably (compared to normal emission) and, hence, allows for more $\vec{P}$ components being nonzero.[47]

In the following, two main types of photoemission setups will be discussed. In the first one, $\vec{k}_\parallel$ lies in a mirror plane of the surface, i.e., $\vec{k}_\parallel$ along $\overline{\mathrm{M}}$-$\overline{\Gamma}$-$\overline{\mathrm{M}}$ [cf. Fig. 1(b)]. Since for $\varphi_e = 90°$ and 270° [$\vec{k}_\parallel = (0,k_y)$], the initial-state ESP is aligned along *x* [Eq. (9)], the light has to be chosen in such a way that the mirror operation $x \to -x$ is retained. For the second type, $\vec{k}_\parallel$ is along $\overline{\mathrm{K}}$-$\overline{\Gamma}$-$\overline{\mathrm{K}}$ [$\vec{k}_\parallel = (k_x,0)$] and only the trivial symmetry operation remains ($\vec{k}_\parallel$ perpendicular to a mirror plane). Therefore, it is not possible to choose incidence direction and polarization of the light in such a way that only P_y is nonzero.

The following results were obtained for linearly and circularly polarized light with a photon energy $\omega = 21.22$ eV ($\mathrm{He_I}$) incident at a polar angle $\vartheta_{ph} = 45°$. Fixing the initial-state energy at E_F, we are concerned with constant initial-energy spectroscopy. Our results hold qualitatively also for other parameters (e.g., polar angle of incidence, initial-state energy, and photon energy).

2. $\overline{\Gamma}$-$\overline{M}$

For $\overline{\mathrm{M}}$-$\overline{\Gamma}$-$\overline{\mathrm{M}}$, from Eq. (9) one obtains that the spin polarization of the initial state is aligned along the *x* axis, $\vec{P} = (\alpha,0,0)$. For off-normally incident *p*-polarized light, the photoelectron spin polarization is normal to the scattering plane [see Ref. 28 for (001) surfaces]. Hence, to probe the initial-state spin polarization for $\overline{\mathrm{M}}$-$\overline{\Gamma}$-$\overline{\mathrm{M}}$ ($\varphi_e = 90°$) one chooses a light incidence within the *yz* plane ($\varphi_{ph} = 90°$ or 270°) which produces a nonzero P_x only.

Scanning the polar angle of emission ϑ_e [Fig. 5(a)], the intensities show four distinct maxima which lie symmetrically around $\overline{\Gamma}$ ($\vec{k}_\parallel = 0$ or $\vartheta_e = 0°$). The inner surface state appears at $\vartheta_e = \pm 4.2°$, the outer at $\vartheta_e = \pm 4.9°$. Bulk contributions to the photocurrent occur for $|\vartheta_e| > 6°$, as can be seen by the very small intensities (compared to the surface-state intensities).

The *x* component of the photoelectron ESP shows distinct minima and maxima at the positions of the surface states [Fig. 5(b)]. The sign of P_x, and hence the sign of α [Eq. (9)], corresponds to those obtained from the spectral-density calculations for the initial state. Even the magnitudes agree well: from Fig. 5 one would deduce $\alpha^{in} \approx -99\%$ and $\alpha^{out} \approx +93\%$, compared to $\alpha^{in} \approx -97\%$ and $\alpha^{out} \approx +93\%$ for the initial states. That intensities and spin polarizations for $\varphi_{ph} = 90°$ and 270° as well as for $\pm\vartheta_e$ differ is attributed to the transition-matrix elements which obviously depend on the direction of light incidence (note in this context the ABC stacking sequence along the [111] direction; see Fig. 1).

The use of *p*-polarized light nicely provides access to the spin polarization of the initial state. For *s*-polarized light, however, this is not completely true, as can be seen in Fig. 6.

In this case, P_x is the only nonzero ESP component, too. For $\varphi_{ph} = 0°$ (that is, for the electric-field vector $\vec{E}$ of the incident radiation parallel to $\vec{y}$), P_x shows the same structure as for *p*-polarized light [solid in Fig. 6(b)]. However, for $\varphi_{ph} = 90°$ ($\vec{E} \| \vec{x}$), one observes the opposite behavior: a positive α^{in} and a negative α^{out} [dashed in Fig. 6(b)]. This finding is a direct manifestation of SOC. Without SOC, an initial-state wave function would be either even or odd under the mirror operation $x \to -x$. The spatial parts for ''spin-up'' ($\uparrow$) and ''spin-down'' ($\downarrow$) would be identical, giving rise to an unpolarized state. However, spin-orbit coupling mixes even and odd initial-state wave functions.[33] Schematically, one can write, for the initial-state wave function,

$$|\Psi\rangle = |\Psi_{even}\rangle\chi^{\tau} + |\Psi_{odd}\rangle\chi^{-\tau}, \quad \tau = \uparrow,\downarrow. \tag{10}$$

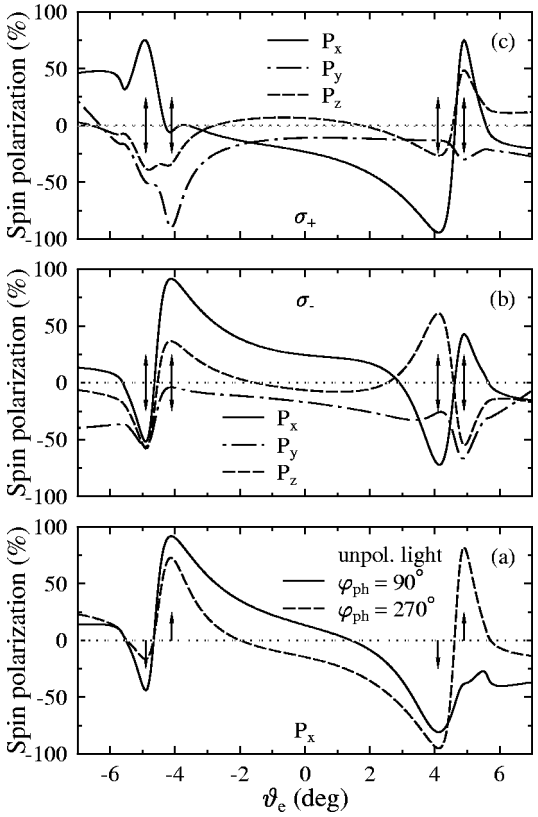

FIG. 7. Spin-resolved photoemission for $\vec{k}_\parallel$ along $\overline{\mathrm{M}}$-$\overline{\Gamma}$-$\overline{\mathrm{M}}$ ($\varphi_e = 90°$, $\omega = 21.22$ eV, $\vartheta_{ph} = 45°$). The vertical arrows mark the surface-state positions. (a) Photoelectron spin polarization along *x* for unpolarized light incident at $\varphi_{ph} = 90°$ (solid) and 270° (dashed) azimuth. (b) and (c) As in panel (a), but for circularly polarized light for positive [σ_-, panel (b)] and negative [σ_+, panel (c)] helicity incident at $\varphi_{ph} = 0°$. The components of the photoelectron spin polarization are differentiated by line styles.

In the dipole approximation, $\vec{E}$ couples to the even spatial part of the initial-state wave function if lying in the mirror plane. This is the case for *p*-polarized light as in Fig. 5 or for *s*-polarized light with $\varphi_{ph} = 0°$. It couples to the odd part if being perpendicular, as is the case for *s*-polarized light incident at $\varphi_{ph} = 90°$. Hence, one can conclude that the even parts of the initial states are dominant (cf. the intensities in Fig. 6: large for $\varphi_{ph} = 0°$, small for $\varphi_{ph} = 90°$; this is confirmed by the angular momentum- and spin-resolved spectral densities) and produce a negative α^{in} and a positive α^{out}. The intensity difference for $\pm\vartheta_e$ can again be attributed to the fcc lattice which is not symmetric with respect to the *xz* plane (*ABC* stacking sequence).

Unpolarized light can be regarded as an incoherent superposition of *s*- and *p*-polarized light. Since, with *s*-polarized light incident within the *yz* plane ($\varphi_{ph} = 90°$), one detects the ''wrong'' ESP [dashed in Fig. 6(b)], a question arises whether unpolarized light provides nevertheless the ''correct'' initial-state ESP. Indeed, P_x shows the $-/+-+/-$ shape [Fig. 7(a)], but the ESP is significantly reduced in absolute value.

The latter can be explained by the smaller intensity for *s*-polarized light than for *p*-polarized light. Hence, using a He_I rare-gas discharge lamp provides information on the sign but not on the magnitude of the initial-state spin polarization.

In order to probe the initial-state $\vec{P}$ with an ''optical orientation,'' one would choose circularly polarized light incident at $\varphi_{ph} = 0°$ or 180°, expecting that mainly P_x would be produced, although all three components of $\vec{P}$ become nonzero for $\vartheta_{ph} \neq 0°$. In this case, the intensities *I* and spin polarizations $\vec{P}$ obey $(I, P_x, P_y, P_z) \rightarrow (I, P_x, -P_y, -P_z)$ when changing φ_{ph} from 0° to 180° and simultaneously reversing the light helicity $\sigma_\pm$ [$I(\sigma_+) \neq I(\sigma_-)$ means that there is circular dichroism in angular distribution]. As is evident from Figs. 7(b) and 7(c) the photoelectron ESP shows a complicated behavior, from which it is almost impossible to conclude on the initial-state spin polarization without prior (theoretical) knowledge.

3. $\overline{\Gamma}$-$\overline{K}$

With $\vec{k}_\parallel$ along $\overline{\mathrm{K}}$-$\overline{\Gamma}$-$\overline{\mathrm{K}}$ ($\varphi_e = 0°$) the only remaining symmetry operation is the trivial one, which yields that all components of the photoelectron ESP are generally nonzero. The initial-state ESP, however, reads $\vec{P} = (0, -\alpha, \beta)$. Thus, a nonzero P_x of the photoelectron would be a direct manifestation of a ESP due to the photoemission process. We have performed photoemission calculations for different light polarizations and incidence directions and found that in most cases the photoelectron spin polarization is hardly to relate to that of the initial state. The most promising results were obtained for *p*-polarized light incident in the *xz* plane ($\varphi_{ph} = 0°$ and 180°). The symmetry of this setup implies certain relations between the intensities *I* and the photoelectron spin polarization $\vec{P}$: simultaneously changing φ_{ph} from 0° to 180° and ϑ_e to $-\vartheta_e$ results in $(I, P_x, P_y, P_z) \rightarrow (I, P_x, -P_y, -P_z)$, that is, P_y and P_z change sign whereas *I* and P_x remain unaffected. Therefore, it is sufficient to discuss only the case $\varphi_{ph} = 0°$. As is evident from Fig. 8, the intensity maxima occur at the same polar angles of emission as along $\overline{\mathrm{M}}$-$\overline{\Gamma}$-$\overline{\mathrm{M}}$ which proves the circular shape of the momentum distribution [Fig. 3(b)].

The dominant component of $\vec{P}$, P_y [solid in Fig. 8(b)], shows a $+/-\text{-}+/-$ shape which agrees well with that of the initial-state spin polarization [Fig. 3(b)]. Further, one finds $|\alpha^{in}| > |\alpha^{out}|$. However, to conclude on the magnitude of α is rather difficult, in particular for α^{out} because of the sizable P_x and P_z. These $\vec{P}$ components are rather large, especially for the outer surface state on which we will focus now. The comparison of the P_z values of 25.7% and 35.3% at $\vartheta_e = -4.9°$ and $+4.9°$ [dashed in Fig. 8(b)], respectively, with those of the initial state (-1.3% and $+1.3\%$) renders it impossible to conclude from the photoelectron spin polarization on that of the surface state. The same holds for P_x [14.8% and 32.0%; dash-dotted in Fig. 8(b)] which is exclusively due to the photoemission process.

Despite this negative but expected result, one can speculate to probe the initial-state P_z by altering the system. First, one needs a spin-polarization effect which produces a dominant P_z. This could be an accomplished by an ''optical ori-

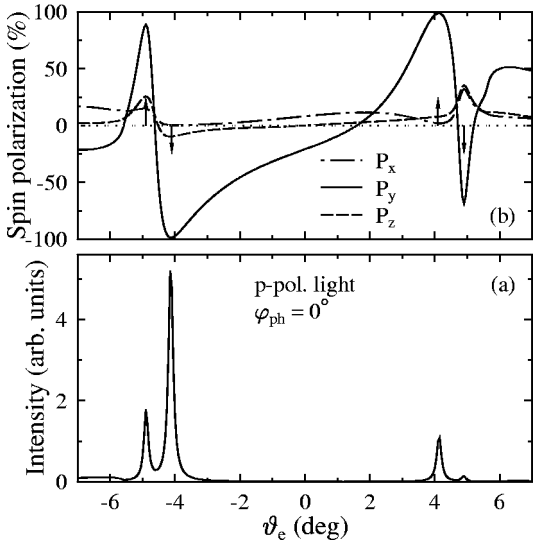

FIG. 8. Spin-resolved photoemission for $\vec{k}_{\parallel}$ along $\overline{\mathrm{K}}$-$\overline{\Gamma}$-$\overline{\mathrm{K}}$ ($\varphi_e = 0°$) and *p*-polarized light ($\omega = 21.22$ eV, $\vartheta_{ph} = 45°$). (a) Intensities for $\varphi_{ph} = 0°$ azimuth of light incidence. (b) Associated photoelectron spin polarization. The vertical arrows mark the surface-state positions.

entation'' with normally incident circularly polarized light, but for off-normal emission the other $\vec{P}$ components are too large to conclude undoubtedly on β. Second, since the small initial-state P_z arises from the corrugation of the surface potential, one might think about increasing the corrugation by covering the surface by an adlayer, e.g., $(\sqrt{3} \times \sqrt{3})$R30°-Xe/Au(111). As reported in Refs. 7 and 48 for Xe/Au(111) and in Ref. 45 for Li/W(110), the spin-orbit splitting of the surface states increased with coverage.

Summarizing, the photoemission calculations prove that it is possible to conclude from the photoelectron spin polarizations on those of the initial *L*-gap surface states, provided the setup is chosen correctly. Otherwise, the photoelectron spin polarization which is brought about by the photoemission process itself obscures the property of interest.

IV. CONCLUDING REMARKS

Our theoretical investigations reveal on one hand a striking similarity between the electronic states in a two-dimensional electron gas (2DEG) with Rashba spin-orbit interaction and the *L*-gap surface states on Au(111). On the other hand, the structure of the Au(111) surface produces a nonzero but small spin-polarization component normal to the surface that is missing in a 2DEG. To probe the spin polarization of the spin-orbit-split surface states by spin- and angle-resolved photoelectron spectroscopy can completely fail if the setup is badly chosen. As a rule of thumb, those setups work best that produce a photoelectron spin polarization aligned along that of the initial state (see, e.g., Refs. 26 and 33). We would like to encourage strongly experiments in order to confirm our theoretical results.

The *L*-gap surface states can be regarded as a source for highly spin-polarized electrons with unique properties. Hence, one can speculate whether the Au(111) surface can be used as a model system for spintronics if brought into contact with magnetic material.

ACKNOWLEDGMENT

We are grateful to Yonko T. Millev for very fruitful discussions.

*Corresponding author. Electronic address: henk@mpi-halle.de

[1] S. LaShell, B.A. McDougall, and E. Jensen, Phys. Rev. Lett. **77**, 3419 (1996).
[2] L. Petersen and P. Hedegård, Surf. Sci. **459**, 49 (2000).
[3] R. Courths, M. Lau, T. Scheunemann, H. Gollisch, and R. Feder, Phys. Rev. B **63**, 195110 (2001).
[4] G. Nicolay, F. Reinert, S. Schmidt, D. Ehm, P. Steiner, and S. Hüfner, Phys. Rev. B **62**, 1631 (2000).
[5] F. Reinert, G. Nicolay, S. Schmidt, D. Ehm, and S. Hüfner, Phys. Rev. B **63**, 115415 (2001).
[6] G. Nicolay, F. Reinert, S. Hüfner, and P. Blaha, Phys. Rev. B **65**, 033407 (2002).
[7] F. Reinert, J. Phys.: Condens. Matter **15**, S693 (2003).
[8] S. Hüfner, *Photoelectron Spectroscopy*, 3rd ed. (Springer, Berlin, 2003).
[9] D. Fujita, K. Amemya, T. Yakabe, H. Nejoh, T. Sato, and M. Iwatsuki, Surf. Sci. **423**, 160 (1999).
[10] E. Rotenberg and S.D. Kevan, Phys. Rev. Lett. **80**, 2905 (1998).
[11] M. Hochstrasser, J.G. Tobin, E. Rotenberg, and S.D. Kevan, Phys. Rev. Lett. **89**, 216802 (2002).
[12] E.I. Rashba, Sov. Phys. Solid State **2**, 1109 (1960).
[13] Y.A. Bychkov and E.I. Rashba, JETP Lett. **39**, 78 (1984).
[14] T.P. Pareek and P. Bruno, Phys. Rev. B **65**, 241305(R) (2002).
[15] J. Schliemann, J. Carlos Egues, and D. Loss, Phys. Rev. Lett. **90**, 146801 (2003).
[16] J. Kessler, *Polarized Electrons*, vol. 1 of *Springer Series on Atoms and Plasmas* (Springer, Berlin, 1985), 2nd ed.
[17] W. Chen, V. Madhavan, T. Jamneala, and M.F. Crommie, Phys. Rev. Lett. **80**, 1469 (1998).
[18] J.P. Perdew and Y. Wang, Phys. Rev. B **45**, 13 244 (1992).
[19] A. Ernst, M. Lüders, W.M. Temmerman, Z. Szotek, and G. van der Laan, J. Phys.: Condens. Matter **12**, 5599 (2000).
[20] P. Weinberger, *Electron Scattering Theory of Ordered and Disordered Matter* (Clarendon Press, Oxford, 1990).
[21] E. Tamura (1996), private communication.
[22] H. Ebert, H. Freyer, A. Vernes, and G.Y. Guo, Phys. Rev. B **53**, 7721 (1996).
[23] J. Henk, T. Scheunemann, S. V. Halilov, E. Tamura, and R. Feder, OMNI2K—*fully relativistic electron spectroscopy calculations* (2000).
[24] J. Braun, Rep. Prog. Phys. **59**, 1267 (1996).
[25] J. Henk, in *Handbook of Thin Film Materials*, edited by H. S. Nalwa (Academic Press, San Diego, 2001), Vol. 2, Chap. 10, p. 479.
[26] R. Feder and J. Henk, in *Spin-Orbit Influenced Spectroscopies of Magnetic Solids*, edited by H. Ebert and G. Schütz, Lecture Notes in Physics, Vol. 466 (Springer, Berlin, 1996), p. 85.
[27] E. Tamura, W. Piepke, and R. Feder, Phys. Rev. Lett. **59**, 934 (1987).

[28] E. Tamura and R. Feder, Europhys. Lett. **16**, 695 (1991).
[29] J. Henk and R. Feder, Europhys. Lett. **28**, 609 (1994).
[30] B. Schmiedeskamp, B. Vogt, and U. Heinzmann, Phys. Rev. Lett. **60**, 651 (1988).
[31] N. Irmer, R. David, B. Schmiedeskamp, and U. Heinzmann, Phys. Rev. B **45**, 3849 (1992).
[32] N. Irmer, F. Frentzen, S.-W. Yu, B. Schmiedeskamp, and U. Heinzmann, J. Electron Spectrosc. Relat. Phenom. **78**, 321 (1996).
[33] J. Henk, T. Scheunemann, S.V. Halilov, and R. Feder, J. Phys.: Condens. Matter **8**, 47 (1996).
[34] A. Fanelsa, E. Kisker, J. Henk, and R. Feder, Phys. Rev. B **54**, 2922 (1996).
[35] W. Kuch, M. Zharnikov, A. Dittschar, K. Meinel, C. Schneider, J. Kirschner, J. Henk, and R. Feder, J. Appl. Phys. **79**, 6426 (1996).
[36] A. Rampe, G. Güntherodt, D. Hartmann, J. Henk, T. Scheunemann, and R. Feder, Phys. Rev. B **57**, 14 370 (1998).
[37] S.D. Ganichev and W. Prettl, cond-mat/0304266 (unpublished).
[38] J. Luo, H. Munekata, F.F. Fang, and P.J. Stiles, Phys. Rev. B **41**, 7685 (1990).
[39] We use atomic Hartree units, $e=\hbar=m=1$ and $c\approx 137.036$.
[40] E. Tamura and R. Feder, Z. Phys. B: Condens. Matter **81**, 425 (1990).
[41] J. Luo, H. Munetaka, F.F. Fang, and P.J. Stiles, Phys. Rev. B **38**, 10 142 (1988).
[42] B. Das, S. Datta, and R. Reifenberger, Phys. Rev. B **41**, 8278 (1990).
[43] G. Engels, J. Lange, T. Schäpers, and H. Lüth, Phys. Rev. B **55**, R1958 (1997).
[44] T. Schäpers, G. Engels, J. Lange, T. Klocke, M. Hollfelder, and H. Lüth, J. Appl. Phys. **83**, 4324 (1998).
[45] E. Rotenberg, J.W. Chung, and S.D. Kevan, Phys. Rev. Lett. **82**, 4066 (1999).
[46] M. Wöhlecke and G. Borstel, in *Optical Orientation*, edited by F. Meier and B.P. Zakharchenya (North-Holland, Amsterdam, 1984).
[47] J. Henk and B. Johansson, J. Electron Spectrosc. Relat. Phenom. **94**, 259 (1998).
[48] F. Forster, G. Nicolay, F. Reinert, D. Ehm, S. Schmidt, and S. Hüfner, Surf. Sci. **532–535**, 160 (2003).